Aalborg Universitet

AALBORG UNIVERSITY

DENMARK

On the Frequency Correction in Temperature-Modulated Differential Scanning Calorimetry of Glass Transition

Guo, Xiaoju; Mauro, J.C.; Allan, D.C.; Yue, Yuanzheng

On the frequency correction in temperature-modulated differential scanning calorimetry of the glass transition

Xiaoju Guo [a,b], John C. Mauro [a,*], Douglas C. Allan [a], Yuanzheng Yue [b,c,**]

[a] Science and Technology Division, Corning Incorporated, Corning, NY 14831, USA
[b] Section of Chemistry, Aalborg University, DK-9000 Aalborg, Denmark
[c] Shandong Key Laboratory for Glass and Ceramics, Shandong Polytechnic University, Jinan 250353, China

ARTICLE INFO

ABSTRACT

Temperature-modulated differential scanning calorimetry (TMDSC) is based on conventional DSC but with a sinusoidally modulated temperature path. Simulations of TMDSC signals were performed for Corning EAGLE XG glass over a wide range of modulation frequencies. Our results reveal that the frequency correction commonly used in the interpretation of TMDSC signals leads to a master nonreversing heat flow curve independent of modulation frequency, provided that sufficiently high frequencies are employed in the TMDSC measurement. A master reversing heat flow curve can also be generated through the frequency correction. The resulting glass transition temperature from the frequency corrected reversing heat flow is thereby shown to be independent of frequency.

© 2012 Elsevier B.V. All rights reserved.

1. Introduction

Heat generation or absorption accompanies most chemical reactions and many important physical transitions such as crystallization, melting, phase separation, glass transition, and relaxation. Differential scanning calorimetry (DSC) is an especially useful technique [1] for measuring the evolution of heat in glass samples as a means for understanding important glass transition and relaxation phenomena. In conventional DSC measurements, the most often used temperature program is a linear heating/cooling thermal path with the total heat flow measured as output.

Temperature-modulated differential scanning calorimetry (TMDSC) is a newer and more advanced technique in which the linear temperature path is modulated with a small periodic temperature perturbation, usually from a sinusoidal drive. The thermal profile in a TMDSC can be heat-cool, iso-temperature-scan, step-scan, or quasi-isothermal [2]. The heat-cool profile is typically used in the study of glass transition behavior. The total heat flow from TMDSC is identical to conventional DSC under the same basic linear thermal profile, i.e., for zero amplitude of the modulating tone. The advantage of TMDSC over conventional DSC is argued as the ability to separate overlapping physical phenomena through deconvolution of the signal into reversing and non-reversing components of the total heat flow [3]. For investigation of glassy systems, the reversing heat flow clearly shows the glass transition range while the non-reversing heat flow is a measure of structural relaxation during the TMDSC scan [3]. Fundamental understanding of the system from TMDSC relies on the ability to analyze the reversing and non-reversing signals correctly. Consequently, proper analysis of TMDSC signals has been a very important topic in the development and application of this technique [4,5].

The reversing component of the heat flow signal can be used to determine a modulation-dependent glass transition temperature [6–10], while the non-reversing heat flow has been widely used in the study of Boolchand intermediate phases in Ge-Se [6–9], As-Se [8–10], Na_2O-SiO_2 [11], Na_2O-GeO_2 [12], and several other glass systems. The range of compositions having a zero or near-zero integrated non-reversing heat flow is termed the "reversibility window" and defines the Boolchand intermediate phase for that system [6–12]. Intermediate phase glasses are topologically optimized glass compositions that usually have an average atomic coordination number ($\langle r \rangle$) near 2.4. According to mean-field topological constraint theory [13–16], when the average coordination value reaches $\langle r \rangle = 2.4$, the number of rigid two- and three-body bond constraints is equal to the total configurational degrees of freedom. This will result in a rigid but unstressed glass structure which sits at the boundary between an underconstrained floppy phase ($\langle r \rangle < 2.4$) and an overconstrained stressed-rigid phase ($\langle r \rangle > 2.4$). The discovery of Boolchand is that the optimized (isostatic) glass is not necessarily represented by just a single composition with $\langle r \rangle$ exactly equal to 2.4. The Boolchand intermediate phase consists of a range of compositions, typically centered in the vicinity of $\langle r \rangle = 2.4$, in which the glass structure self-organizes to obtain an isostatic stress-free condition. However, some controversies have arisen regarding the validity of the TMDSC measurement and the

existence of the Boolchand intermediate phase. One controversy is in regard to the structure dependence of the intermediate phase in the TMDSC measurement [17]. A second controversy relates to the impact of modulation frequency on the TMDSC results and the resulting physical implications [18]. Here we will focus on the second issue, i.e., the influence of frequency on the TMDSC results and analysis.

The frequency dependence of non-reversing heat flow and glass transition temperature from TMDSC have been noted experimentally [19] and also in simulated experimental scans [20,21]. In Chen et al.'s aging study of selenide glasses, the non-reversing enthalpy is reported as frequency corrected [19]. Generally speaking, in order to do the frequency correction for the non-reversing enthalpy calculation, a cooling scan with the same linear cooling rate overlapped with the same periodic perturbation is required following the initial heating. By subtracting the non-reversing enthalpy in the cooling cycle from the non-reversing enthalpy measured in the heating cycle, a corrected non-reversing enthalpy is obtained. It is expected that we should be able to obtain a universal non-reversing enthalpy after the frequency correction for any frequency of the periodic perturbation in TMDSC. However, the ability to test this hypothesis experimentally is severely limited by the range of frequencies accessible in laboratory TMDSC equipment: at high frequencies the experiment is limited by heat transfer of the sample, and at low frequencies the experiment is limited by the long times required in order to keep sufficient modulation periods in the glass transition range.

To overcome these limitations and study the validity of the frequency correction, here we will present the results of TMDSC "virtual experiments" on Corning EAGLE XG glass. The frequency range in the simulated TMDSC experiment can be much wider than in experiment since there is no limitation on heat transfer from the sample to the environment. The simulated results demonstrate that the frequency correction can produce a universal non-reversing heat flow given that a sufficient number of modulation periods occur during the glass transition range of the sample.

2. Modeling procedure

The simulated TMDSC experiments for EAGLE XG glass are performed using the same approach as used previously in our work on fictive temperature [22]. The enthalpy relaxation follows a stretched exponential decay function [23–25], which is expressed as a Prony series of 12 simple exponential terms for convenience of the numerical solution. The dimensionless stretching exponent is 3/7, which has been demonstrated to be intrinsic for enthalpy relaxation in homogeneous glass in three dimensions [26–29]. The relaxation time is proportional to the nonequilibrium shear viscosity given by the Mauro–Allan–Potuzak (MAP) [30] model, where the equilibrium viscosity contribution is expressed by the Mauro–Yue–Ellison–Gupta–Allan (MYEGA) equation [31]. All of the parameters needed in the model for EAGLE XG glass are published by Mauro et al. [30].

The glass is formed by quenching as a pre-thermal history and is then subjected to two TMDSC upscans with one intermediate downscan. As shown in Fig. 1(a), the starting temperature of the simulated TMDSC scan is 25 °C. The maximum temperature reached during both upscans is 1000 °C, which is well above the glass transition temperature of $T_g = 735.7$ °C (the temperature where the equilibrium viscosity is 10^{12} Pa-s). The linear heating/cooling rate is 1 °C/min, and the amplitude of the periodic sinusoidal perturbation is 5 °C. The modulation frequency is varied from 0.0005 to 0.01 Hz, corresponding to a range of periods from 100 to 2000 s. The as-formed glass has a quenched thermal history as described in Ref. [30]. During the first upscan, this quenched glass is heated to an equilibrium state (1000 °C) and then cooled back to 25 °C. A second, identical upscan is then performed for this "rejuvenated" glass. The output heat flow of the simulated experiment has the same feature as the modulated heat flow signal, $\dot{H}_{TMDSC}$, shown in Fig. A1(b) of Ref. [19]. Then the average
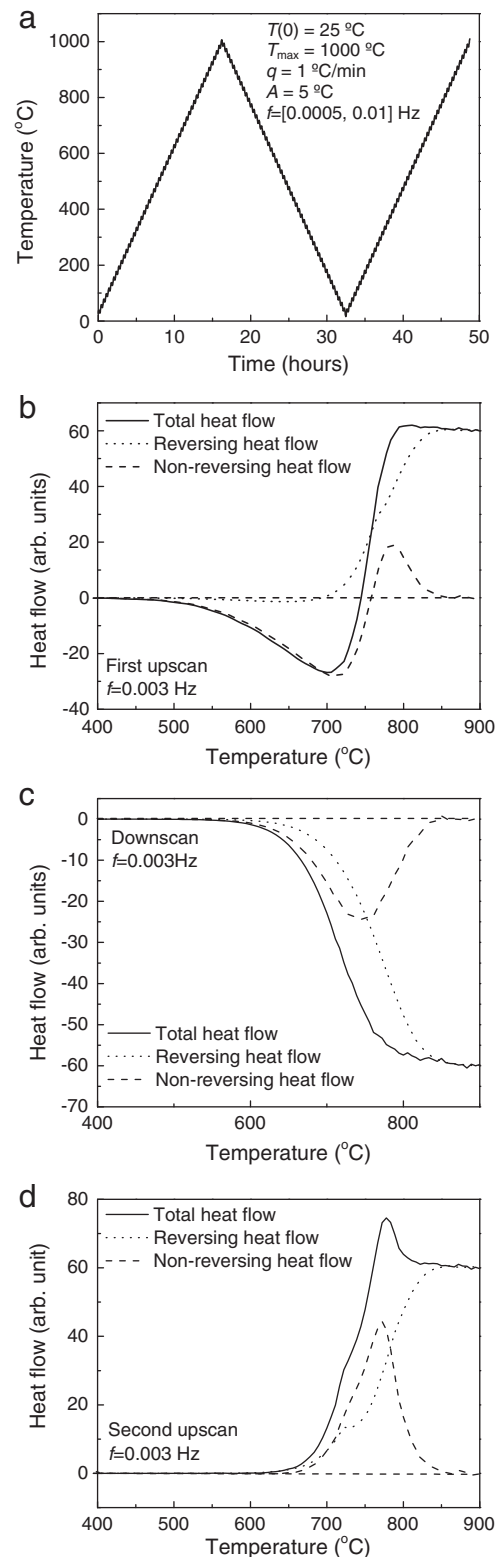
Fig. 1. The thermal path and analyzed total heat flows from the simulation. (a) Thermal path setting up in TMDSC simulation, the starting temperature 25 °C, maximum temperature reached at both upscans 1000 °C, the basic linear heating/cooling rate 1 °C/min, the amplitude of the periodic sinusoidal perturbation 5 °C, and modulation frequencies (f) ranged from 0.0005 to 0.01 Hz; the total heat flow, reversing and non-reversing heat flow for quenched EAGLE XG at $f = 0.003$ Hz: (b) first upscan; (c) downscan; (d) second upscan.

heat flow (total heat flow) and amplitude are generated by Fourier transformation. Then the total heat flow is decomposed to reversing heat flow and non-reversing heat flow for the two upscans and the

downscan following the appendix of Ref. [19]. In Fig. 1(b)–(d), the heat flows from frequency equal to 0.003 Hz is shown as an example. In all of the calculations, the solid (vibrational) heat flow has been subtracted from the total heat flow, such that only the excess (primarily configurational) heat flow is showing in all the figures in this report.

3. Results

After separating the non-reversing part from the total heat flows for different modulation frequencies, we perform the frequency correction for the non-reversing heat flow by adding the (negative) non-reversing heat flow during cooling to the non-reversing heat flow calculated on heating. Fig. 2 shows an example of the frequency correction for both the quenched and rejuvenated glasses using a modulation frequency of 0.003 Hz. The final non-reversing heat flows with and without the frequency correction are plotted in Fig. 3(a) and (b) for the quenched glass and Fig. 3(c) and (d) for the rejuvenated glass over the full range of modulation frequencies. The solid lines in these figures show the continuous non-reversing heat flow for each frequency >0.001 Hz, and the dotted lines show the results for the two lowest modulation frequencies (0.0005 and 0.001 Hz). When the modulation frequency is too low for the given linear heating/cooling rate, there are insufficient thermal cycles of the periodic perturbation within the glass transition range. This results in an effective local heating rate in the TMDSC that is significantly different from the intended linear upscan rate. Finally, as we can see the curves obtained at 0.0005 Hz and 0.001 Hz in Fig. 3(a) and (c), the measured heat flow will deviate from the relative higher frequencies. As shown in Fig. 3(b) and (d), there is a clear departure of the two lowest frequencies even after the frequency correction. For the rejuvenated glass, we obtain wholly overlapped non-reversing heat flows from 0.003 to 0.01 Hz. However, the appropriate lower bound on frequency for the overlaid non-reversing heat flow seems to have increased to 0.006 Hz for the quenched glass.
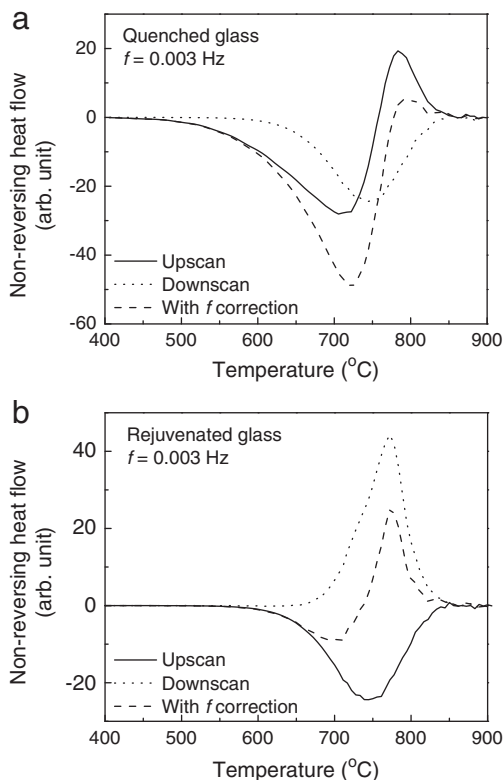
Fig. 2. The non-reversing heat flow in upscan and down scan and with frequency (*f*) correction at *f* = 0.003 Hz: (a) quenched glass; (b) rejuvenated glass.

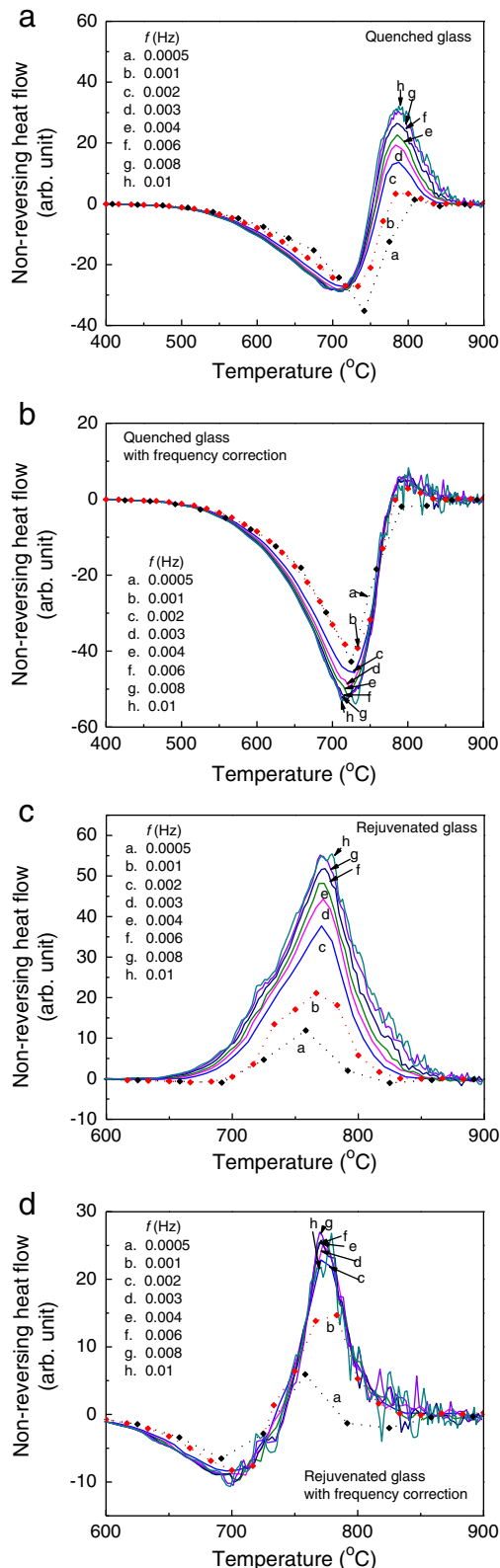**Fig. 3.** The non-reversing heat flow at modulation frequencies (*f*) from 0.0005 to 0.01 Hz: (a) quenched glass; (b) quenched glass with *f* correction; (c) rejuvenated glass; (d) rejuvenated glass with *f* correction.

4. Discussion

As already described, the non-reversing heat flow is calculated by subtracting the reversing heat flow from the total heat flow. Thus, the

frequency correction of non-reversing heat flow also entails a frequency correction in the reversing heat flow. But why should we expect that addition of the non-reversing heat flow in cooling with that during heating can produce a frequency independent non-reversing heat flow? The basic mathematical relation among total heat flow, reversing heat flow, and non-reversing heat flow in heating can be expressed as

$$\dot{H}_{h,total} = \dot{H}_{h,rev} + \dot{H}_{h,non}, \tag{1}$$

where $\dot{H}_{h,total}$ is the total heat flow during heating, $\dot{H}_{h,rev}$ the reversing heat flow during heating, and $\dot{H}_{h,non}$ the non-reversing heat flow on heating. The frequency correction of non-reversing heat flow can be made by introducing the non-reversing heat flow in the cooling cycle, $\dot{H}_{c,non}$, into Eq. (1), i.e., by using this relation

$$\dot{H}_{h,total} = \left(\dot{H}_{h,rev} - \dot{H}_{c,non}\right) + \left(\dot{H}_{h,non} + \dot{H}_{c,non}\right)$$
$$= \dot{H}_{h,rev}^{f} + \left(\dot{H}_{h,non} + \dot{H}_{c,non}\right), \tag{2}$$

where $\dot{H}_{h,rev}^{f} = \dot{H}_{h,rev} - \dot{H}_{c,non}$ is the frequency corrected reversing heat flow given by

$$\dot{H}_{h,rev}^{f} = \left(\dot{H}_{h,rev} + \dot{H}_{c,rev}\right) - \dot{H}_{c,rev} - \dot{H}_{c,non}$$
$$= \left(\dot{H}_{h,rev} + \dot{H}_{c,rev}\right) - \dot{H}_{c,total}. \tag{3}$$

Here $\dot{H}_{c,rev}$ is the reversing heat flow in the cooling cycle, and $\dot{H}_{c,total}$ is the total heat flow in cooling. The frequency corrected non-reversing heat flow is therefore

$$\dot{H}_{h,non}^{f} = \dot{H}_{h,total} - \dot{H}_{h,rev}^{f} = \dot{H}_{h,total} + \dot{H}_{c,total} - \left(\dot{H}_{h,rev} + \dot{H}_{c,rev}\right). \tag{4}$$

It is well known that the total heat flow in heating/cooling is not dependent on modulation frequency. Thus, the frequency corrected non-reversing heat flow is only dependent on the reversing heat flow during heating and cooling. If the sum of the reversing heat flows from heating and cooling is not frequency dependent, the non-reversing heat flow after frequency correction will also be independent of frequency. The frequency correction of the non-reversing heat flow for the quenched and rejuvenated glass reveals a lower limit to the range of frequencies over which a master non-reversing heat flow curve can be generated as shown in Fig. 3(a)–(d). The frequency corrections for the reversing heat flow of quenched and rejuvenated glass are shown in Fig. 4(a) and (b). As shown in Ref. [19], a higher frequency pushes the reversing heat flow signal to higher temperature, and this effect is also shown in the inset of Fig. 4(a). The fully overlapped reversing heat flow in Fig. 4(a) for the rejuvenated glass clearly shows that the frequency correction can generate a reversing heat flow that is independent of modulation frequency. However, the frequency correction of reversing heat flow shown in Fig. 4(b) for the quenched glass gives a range of proper frequencies for getting a master heat flow curve compared to that for the rejuvenated glass. Here the minimum frequency required to obtain a frequency independent curve after the correction is 0.006 Hz, which corresponds to 48 cycles in the glass transition range.

A useful kinetic property of the glass system that can be obtained from the reversing heat flow in TMDSC is the glass transition temperature (T_g). From the heat flow or the heat capacity curve measured by conventional DSC, three different points on the glass transition peak could be identified as T_g [32]: (1) the onset point, i.e., the temperature at which the transition from the glassy state to the supercooled liquid state begins; (2) the end point (T_e), i.e., the temperature at which the supercooled liquid state has been fully reached; and (3) the inflection point, i.e., the temperature at which the slope of the heat capacity curve is a maximum. This inflection point is the standard glass
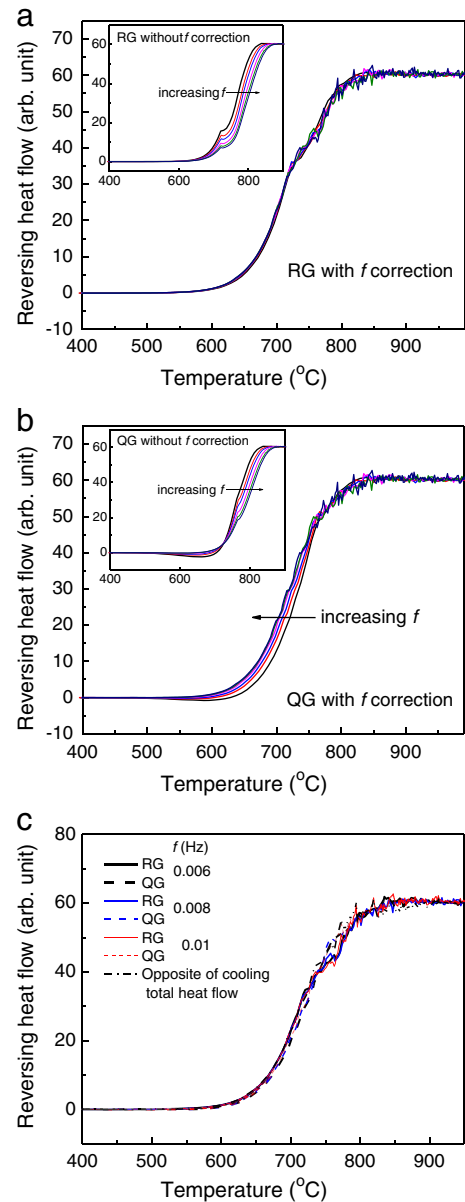

Fig. 4. The reversing heat flow with frequency (f) correction: (a) rejuvenated glass (RG) showing a master curve for $f = 0.002, 0.003, 0.004, 0.006, 0.008, 0.01$ Hz; (b) quenched glass (QG) showing a master curve for $f = 0.002, 0.003, 0.004, 0.006, 0.008, 0.01$ Hz; (c) rejuvenated glass (RG) and quenched glass (QG) for $f = 0.006, 0.008, 0.01$ Hz and the opposite of the total heat flow in cooling. (The heat flow in cooling is exothermic, other than endothermic in heating. In order to see how comparable with endothermic heat flow, the opposite of the total heat flow in cooling is drawn here.)

transition temperature defined by ASTM [33]. A similar approach can be used to determine the glass transition temperature from the reversing heat flow in TMDSC. In Ref. [19], the glass transition temperature is determined as the inflection point of the rapidly rising curve of heat flow in the glass transition range. Here we also use the inflection point as the glass transition temperature. However, the reversing heat flow of glass transition is frequency dependent, where a higher frequency will push the glass transition to higher temperature. The total heat flow from TMDSC is identical to the output of conventional DSC. Thus, in the case of the rejuvenated EAGLE XG glass, the glass transition temperature from conventional DSC (total heat flow) is about 726 °C at heating rate of 1 °C/min. Without the frequency correction, the T_g values are distributed between 764 and 795 °C in the frequency range from 0.002 to 0.01 Hz as shown in the inset of Fig. 4(a). After applying the frequency correction, the common glass transition temperature is

713 °C. The temperature corresponding to 10^{12} Pa-s viscosity for EAGLE XG glass is 735.7 °C. Following the MYEGA viscosity model and the parameters listed in Ref. [30] for EAGLE XG, viz., $\log(\eta_\infty) = -3$, $T_g = 735.7$ °C, and $m = 32.5$, the corresponding equilibrium viscosity values at the above temperatures are: $10^{12.8}$ Pa-s (at 713 °C), $10^{12.3}$ Pa-s (at 726 °C), $10^{11.1}$ Pa-s (at 764 °C), and $10^{10.3}$ Pa-s (at 795 °C). The glass transition is well known as a kinetic property, i.e., it is heating/cooling rate dependent. If we take the linear heating rate 1 °C/min in TMDSC as the heating rate, the glass transition temperature should be a unique value. Thus, either the value from the total heat flow or the value from the frequency corrected reversing heat flow could be selected as glass transition temperature. But since these two values have an offset of 13 °C, which value should be used as the correct glass transition temperature? To answer this question, we must compare these values to the glass transition temperature determined upon cooling from the liquid state, which should be considered as the real glass transition temperature. According to the calculation of frequency correction for reversing heat flow in heating, the frequency corrected reversing heat flow during cooling is the sum of the measured reversing heat flow and the non-reversing heat flow during cooling, which is identical to the total heat flow in cooling. Thus, the glass transition temperature in cooling is determined only by the total heat flow. Finally, the glass transition temperature is found to be 713 °C when the linear cooling rate is 1 °C/min, which is exactly the value obtained from the frequency corrected reversing heat flow.

We now further check the glass transition temperature of the quenched EAGLE XG glass. The glass transition temperature of quenched EAGLE XG glass cannot be obtained from the total heat flow as shown in Fig. 1(b). As shown in Fig. 4(b), the glass transition temperature from reversing heat flow is also frequency dependent before the frequency correction. It shows a similar trend as with the rejuvenated glass in Fig. 4(a): the higher the modulation frequency, the higher the temperature at the inflection point of reversing heat flow curve. After the frequency correction, the opposite trend is observed, i.e., the reversing heat flow curve for the low frequency appears at the high temperature side. However, the reversing heat flow curves for 0.006, 0.008 and 0.01 Hz are fully overlapped. From the master curve for the reversing heat flow in Fig. 4(b), the inflection point is 719 °C, i.e., 6 °C higher than that of the rejuvenated glass. The frequency corrected reversing heat flow curves of both quenched glass and rejuvenated glass for 0.006, 0.008, and 0.01 Hz are presented in Fig. 4(c). All six curves are almost fully overlapped, indicating that glasses with the same composition but with different pre-TMDSC thermal histories (quenched and 1 °C/min cooling) should have a similar glass transition temperature if the same heating rate is used in the TMDSC measurement.

According to topological constraint theory, the glass transition occurs when a sufficient number of constraints in the network become rigid. For oxide glasses the vitrification process is typically controlled by angular constraints in the network [34–38]. In DSC/TMDSC measurements, when the glass transition occurs during upscan, the network is becoming more floppy. The glass structure is influenced by the thermal history of the glass, e.g. cooling rate and annealing time. However, the very narrow range of glass transition temperatures obtained for the quenched and rejuvenated glass at the same TMDSC heating rate implies that the structure of the constraint controlling glass transition is not significantly affected by the cooling rate. This is in good agreement with our DSC study of the physical aging of hyperquenched glass fibers, where the glass transition temperatures of hyperquenched and annealed hyperquenched glasses are found to be independent of thermal history [39]. This finding can now be directly verified through the measurement of glass transition temperature using the frequency corrected reversing heat flow in TMDSC. The heat flow in the cooling cycle is exothermic. In order to compare with the endothermic heat flow in the heating cycles, the opposite of the total heat flow in the cooling cycle of

TMDSC measurement is also included in Fig. 4(c). This clearly shows that the opposite of the total heat flow during downscan lies on top of the frequency corrected reversing heat flow of the rejuvenated glass. Thus, the glass transition temperature obtained from the frequency corrected reversing heat flow in TMDSC is close to that from the cooling cycle of conventional DSC. Concerning the specific case of T_g determination, the TMDSC approach is more complicated than the conventional DSC approach using a single cooling cycle. However, the conventional DSC may not be a good approach for determining the real glass transition temperature since the glass transition range is overlapped with simultaneous enthalpy relaxation.

Besides the T_g determination from frequency corrected reversing heat flow, another application of TMDSC is determination of the enthalpy recovery of a glass during aging, i.e., the area enclosed in frequency corrected non-reversing heat flow curves of the quenched and rejuvenated glass. This area is taken as the enthalpy difference between the quenched and rejuvenated glass during the TMDSC upscans [19]. The non-reversing heat flows after frequency correction of quenched and rejuvenated glasses are shown in Fig. 5. The total heat flows of both quenched and rejuvenated glasses are represented by the green curves in the same figure. The area enclosed by the total upscan heat flows of quenched and rejuvenated glasses is taken as the total aging enthalpy during conventional DSC measurement. In the case of TMDSC, the area enclosed by non-reversing heat flows after applying the frequency correction to the quenched and rejuvenated glasses is also taken as the total aging enthalpy. Therefore, both techniques should yield the same value for the aging enthalpy. For our simulation of EAGLE XG, the area enclosed by the green total heat flow in Fig. 5 is 6114 arbitrary units, while the area enclosed by the frequency-correction non-reversing heat flow from TMDSC is 6116 arbitrary units (here selecting 0.01 Hz as the modulation frequency). The excellent agreement between these two results indicates that non-reversing heat flow after frequency correction is a good representation of the total aging effect.

5. Conclusions

From the TMDSC simulations of EAGLE XG glass, it is found that the frequency correction of non-reversing heat flow gives a master curve for both quenched and rejuvenated glass provided that a sufficient number of modulation cycles occur during the glass transition. This minimum frequency is dependent not only on the measurement parameters such as linear heating/cooling rate and frequency and amplitude of the modulation, but also on the previous thermal history of the glass before the TMDSC measurement. The frequency corrected reversing heat flow of the rejuvenated glass gives an identical glass transition temperature as that obtained during the cooling cycle.
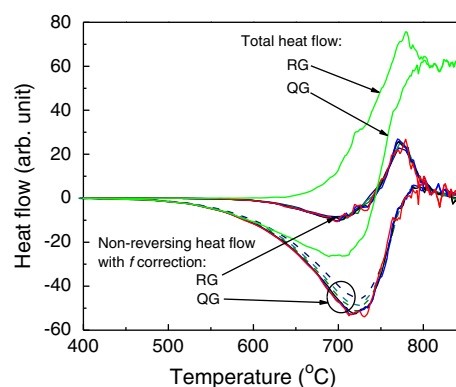
Fig. 5. The area enclosed by the non-reversing heat flow master curves of quenched glass (QG) and rejuvenated glass (RG) for frequencies (f): 0.002, 0.003, 0.004, 0.006, 0.008, 0.01 Hz, comparing with the area enclosed by the total heat flow curves of QG and RG.

In addition, frequency corrected reversing heat flow gives a nearly identical glass transition temperature for both the quenched glass and rejuvenated glass. This implies that the topological constraint governing the glass transition is insensitive to thermal history. The enthalpy calculated by the frequency corrected non-reversing heat flow of quenched and rejuvenated glass is identical to the total aging enthalpy from the total heat flow.

Acknowledgments

References

[1] G.W.H. Höhne, W.F. Hemminger, H.-J. Flammersheim, Differential Scanning Calorimetry, 2nd ed. Springer, Berlin, 2003.
[2] R.A. Shanks, L.M.W.K. Gunaratne, J. Therm. Anal. Calorim. 104 (2011) 1117.
[3] E. Verdonck, K. Schaap, L.C. Thomas, Int. J. Pharm. 192 (1999) 3.
[4] S.X. Xu, Y. Li, Y.P. Feng, Thermochim. Acta 343 (2000) 81.
[5] Z. Jiang, C.T. Imrie, J.M. Hutchinson, Thermochim. Acta 387 (2002) 75.
[6] P. Boolchand, X. Feng, W.J. Bresser, J. Non-Cryst. Solids 293–295 (2001) 348.
[7] S. Chakravarty, D.G. Georgiev, P. Boolchand, M. Micoulaut, J. Phys. Condens. Matter 17 (2005) L1.
[8] P. Boolchand, D.G. Georgiev, M. Micoulaut, J. Optoelectron. Adv. Mater. 4 (2002) 823.
[9] P. Boolchand, D.G. Georgiev, B. Goodman, J. Optoelectron. Adv. Mater. 3 (2001) 703.
[10] D.G. Georgiev, P. Boolchand, M. Micoulaut, Phys. Rev. B 62 (2000) R9228.
[11] Y. Vaills, T. Qu, M. Micoulaut, F. Chaimbault, P. Boolchand, J. Phys. Condens. Matter 17 (2005) 4889.
[12] K. Rompicharla, D.I. Novita, P. Chen, P. Boolchand, M. Micoulaut, W. Huff, J. Phys. Condens. Matter 20 (2008) 202101.
[13] J.C. Phillips, J. Non-Cryst. Solids 34 (1979) 153.
[14] J.C. Phillips, J. Non-Cryst. Solids 43 (1981) 37.
[15] M.F. Thorpe, J. Non-Cryst. Solids 57 (1983) 355.
[16] J.C. Phillips, M.F. Thorpe, Solid State Commun. 53 (1985) 699.
[17] G. Yang, B. Bureau, T. Rouxel, Y. Gueguen, O. Gulbiten, C. Roiland, E. Soignard, J.L. Yarger, J. Troles, J.-C. Sangleboeuf, P. Lucas, Phys. Rev. B 82 (2010) 195206.
[18] P. Lucas, E.A. King, O. Gulbiten, J.L. Yarger, E. Soignard, B. Bureau, Phys. Rev. B 80 (2009) 214114.
[19] P. Chen, P. Boolchand, D.G. Georgiev, J. Phys. Condens. Matter 22 (2010) 065104.
[20] S.L. Simon, Thermochim. Acta 374 (2001) 55.
[21] S.L. Simon, G.B. McKenna, Thermochim. Acta 348 (2000) 77.
[22] X.J. Guo, M. Potuzak, J.C. Mauro, D.C. Allan, T.J. Kiczenski, Y.Z. Yue, J. Non-Cryst. Solids 357 (2011) 3230.
[23] R. Kohlrausch, Pogg. Ann. Phys. 12 (1847) 393.
[24] R. Kohlrausch, Ann. Phys. Chem. 167 (1854) 179.
[25] G. Williams, D.C. Watts, Trans. Faraday Soc. 66 (1970) 80.
[26] J.R. Macdonald, J.C. Phillips, J. Chem. Phys. 122 (2005) 074510.
[27] J.C. Phillips, J. Non-Cryst. Solids 352 (2006) 4490.
[28] J.C. Phillips, Rep. Prog. Phys. 59 (1996) 1133.
[29] M. Potuzak, R.C. Welch, J.C. Mauro, J. Chem. Phys. 135 (2011) 214502.
[30] J.C. Mauro, D.C. Allan, M. Potuzak, Phys. Rev. B 80 (2009) 094204.
[31] J.C. Mauro, Y.Z. Yue, A.J. Ellison, P.K. Gupta, D.C. Allan, Proc. Natl. Acad. Sci. U. S. A. 106 (2009) 19780.
[32] D. Simatos, G. Blond, G. Roudaut, D. Champion, J. Perez, A.L. Faivre, J. Therm. Anal. 47 (1996) 1419.
[33] ASTM Standard Method E (1991) 1356–1391.
[34] P.K. Gupta, J.C. Mauro, J. Chem. Phys. 130 (2009) 094503.
[35] J.C. Mauro, P.K. Gupta, R.J. Loucks, J. Chem. Phys. 130 (2009) 234503.
[36] M.M. Smedskjaer, J.C. Mauro, S. Sen, Y.Z. Yue, Chem. Mater. 22 (2010) 5358.
[37] M.M. Smedskjaer, J.C. Mauro, Y.Z. Yue, Phys. Rev. Lett. 105 (2010) 115503.
[38] M.M. Smedskjaer, J.C. Mauro, R.E. Youngman, C.L. Hogue, M. Potuzak, Y.Z. Yue, J. Phys. Chem. B 115 (2011) 12930.
[39] X.J. Guo, J.C. Mauro, M. Potuzak, Y.Z. Yue, J. Non-Cryst. Solids 358 (2012) 1356.